Article

Solvent-Free Aldol Condensation of Cyclopentanone with Natural Clay-Based Catalysts: Origin of Activity & Selectivity

Xianglong Meng [1], Hui Su [2], Ranran Song [2], Jianzheng Su [1] and Junjie Bian [2,*]

[1] State Energy Center for Shale Oil Research and Development, SINOPEC, Beijing 100728, China
[2] School of Chemistry and Chemical Engineering, Ocean University of China, Qingdao 266100, China
*   Correspondence: junjiebian@ouc.edu.cn; Tel.: +86-(532)-66782502

Abstract: The conversion of biomass resources into high-value fuels and chemicals using thermochemical methods has become an attractive method of energy utilization. In this study, natural minerals were used as raw materials; the acidic sites were introduced by ball-milling modification, and the aldol condensation reaction of the biomass-based cyclopentanone molecule was carried out under solvent-free conditions. It was found that the SO_3H-APG catalyst—with strong medium-based sites when the -SO_3H loading was 4 mmol/g—exhibited excellent acid–base co-activation effects and a significant catalytic effect in the cyclopentanone condensation reaction. The optimization of the reaction conditions showed that the conversion of cyclopentanone reached 85.53% at the reaction temperature of 150 °C and reaction time of 4 h. The selectivity of the dimer and trimer was 69.04% and 28.41%, respectively. The investigation of the cyclopentanone condensation mechanism and kinetic analysis showed that the acid–base presence of an acid–base bifunctional catalyst was important to facilitate the condensation reaction. This research route is in line with the concept of sustainable green production and also provides a promising pathway for catalyst design and the synthesis of long-chain hydrocarbons.

Keywords: cyclopentanone; aldol condensation; acid–base bifunctional catalyst; solvent-free

1. Introduction

The utilization of renewable biomass resources to produce biofuels and high-value chemicals has become an important measure to solve the problem of resource consumption [1–6], in addition to having great significance in the implementation of the strategic tasks of carbon peaking and carbon neutrality. The thermochemical transformation of biomass resources with abundant sources can generate important chemicals such as acids, aldehydes, ketones, and furans, which are widely used in pharmaceutical, fragrance, cosmetics, and high-density fuel fields, among others [7–12]. Cyclopentanone has been extensively studied due to its ability to achieve carbon chain growth through self-condensation and cross-condensation reactions [13,14]. Dimer 2-cyclopentylidene-cyclopentan-1-one (C10)—generated under the catalysis of an acid or base—is a kind of crucial chemical intermediate, which can be used not only as a fragrance additive in everyday chemical products and foods [15], but also as a precursor of high-density fuel oils in aerospace engineering and rockets [16].

The conversion of biomass platform compounds into multi-carbon intermediates is achieved by C–C coupling reactions to growing carbon chains, and is then followed by hydrodeoxygenation to obtain liquid alkane fuels with a high energy density [17,18]. At present, aldol condensation is the most widely used and promising method [19,20]. Aldol condensation reaction is an effective C–C bonding reaction, and some short carbonyl compounds (e.g., ketones, aldehydes) derived from the biomass are particularly suitable for C–C coupling, upgrading and making catalytic upgrading easier for use on fuels and chemicals [21–23]. The cyclopentanone can easily undergo an aldol condensation reaction

to generate α- and β-unsaturated dimer ketones, which can be generated by hydrodeoxygenation to produce combustible molecules [24]. The dimer (C10) and the trimer (C15) are both valuable chemicals, and the latter is also routinely used as a precursor to diesel-grade products via hydrogenation [23]. This study focused on dimmer yield under solvent-free conditions to achieve the acid–base catalytic conversion of cost-efficient catalysts.

Since the steric hindrance of cyclopentanone makes its self-aldol condensation reaction difficult to achieve, it is necessary to add a catalyst with high catalytic activity to promote the reaction [25]. At present, in addition to the use of homogeneous catalysts such as KOH and NaOH, many efforts have been made by scholars around the world to develop active multiphase catalysts [26–29]. The use of acid–base bifunctional catalysts has achieved good results in the aldol condensation reaction of cyclopentanone. The Ni-Mg-Al-O/AC bifunctional catalyst was prepared for cyclopentanone aldol condensation and hydrodeoxygenation reaction to obtain high-performance jet fuel [30]. In addition, acid–base bifunctional catalysts with different acid strengths were used by fixing the basic amino groups and changing the type of acid groups, and it has been found that weak acid groups significantly improved the aldol condensation reaction activity [31]. Using aldol condensation over a modified chitosan catalyst and subsequent hydrodeoxygenation, Q. Zhang's team created long-chain alkanes. A high level of C15 production is the consequence of the complementary effects of the amino and NaOH [32]. A. Amarasekara tested the aldol dimerization of levulinic acid over solid acid catalysts—including Amberlyst-15, SiO_2-SO_3H, Carbon-SO_3H, and $H_3PW_{12}O_{40}$—at 110–130 °C, and also discussed the possibility of the reuse of catalysts [33]. The main advantage of acid–base bifunctional catalysts was their capability to have their so-called synergistic catalysis be tailored, which relies on the synergistic effect of the acid–base sites to facilitate the hydroxyl aldol condensation reaction. Through the aldol dimerization of levulinic acid, M. Paniagua produced bio-jet fuel precursors without solvents on sulfonic SBA-15 Silicas [34]. Thus, cost-effective acid–base solid catalysts would be designed and fabricated, and solvent-free condensation would be a better approach for the dimerization of cyclopentanone.

In this paper, a new method was proposed for the preparation of acid–base bifunctional catalysts using natural clay minerals modified by ball milling. The mechano-chemical approach conforms to the concept of green chemistry and economic efficiency, and it is suitable for the mass production of inexpensive catalysts [35,36]. Natural attapulgite contained Mg^{2+}, Al^{3+} and their oxides, which can be used as basic sites, and the precursor was grafted with -SO_3H group by ball milling to introduce acidic sites. The optimization of reaction conditions for the cyclopentanone aldol condensation was carried out on an electric heating jacket with a reflux device and magnetic stirring, and its catalytic properties were studied in solvent-free conditions. Because the use of organic solvents produced environmental waste and high energy consumption to separate the reaction mixture. Thus, the use of a solvent-free system was more conducive to efficient reactions. The construction of environmentally friendly and efficient acid–base bifunctional catalysts provides a new idea for the "one-pot" preparation of biofuel from biomass-based platform compounds in a solvent-free system.

2. Results and Discussion

2.1. Characterization of the Synthesized SO_3H-APG

The morphology and microstructure of the clay-based catalysts were observed by transmission electron microscopy (TEM) and scanning electron microscopy (SEM) as shown in Figure 1. It can be observed that the catalyst has a rod-like structure and the crystals are stacked with each other. It could also be clearly seen from the EDX pattern that Si, Al, Mg and Ca elements were distributed in the SO_3H-APG catalyst and the abundant basic sites on APG originated from relatively high Mg content.
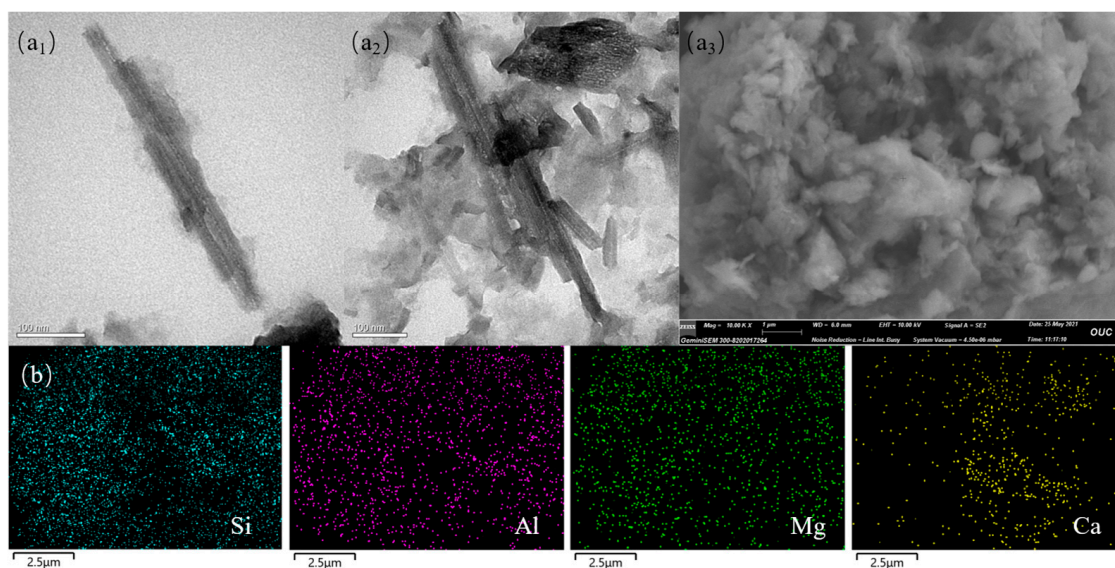
Figure 1. TEM (**a1**,**a2**) and SEM (**a3**) and elements mapping (**b**) of SO_3H-APG catalyst of (**a3**).

The FT-IR spectrum of the SO_3H-APG catalyst was shown in Figure 2a, from which it can be seen that the absorption peaks at 795 cm^{-1} and 1045 cm^{-1} were attributed to the stretching vibration of the Si-O-Si bond [37], except for the characteristic peaks of the clay at 455 cm^{-1} and 520 cm^{-1} (bending vibration of the Si-O bond), and the peaks at 1065 cm^{-1} and 1172 cm^{-1} were attributed to the stretching vibration of the O=S=O bond (-SO_3H) [38], indicating that the -SH has been oxidized to -SO_3H and successfully grafted to the APG surface. The bending vibration absorption band of the hydroxyl group at 1634 cm^{-1}, and the absorption peak at 2943 cm^{-1} were due to the stretching vibration of the C-H bond in the methylene group. The introducing sulfonic acid group did not destroy the crystal structure of attapulgite as also seen in the XRD spectrum (Figure S2).

The N_2 adsorption–desorption isotherms of the SO_3H-APG catalyst and the pore size distribution curves were displayed in Figure 2b. It can be seen that the catalysts exhibited relatively complete adsorption hysteresis curves, indicating that the samples had typical properties of mesoporous materials, and the pore sizes were mainly concentrated around 3.83 nm (Table S4). The grafting of the sulfonic acid group on the outer surface made the catalyst processing good accessibility to active centers, and the larger specific surface area and pore size would help to expose more acid and base sites, thus facilitating the catalytic conversion of the cyclopentanone condensation.

Clinoptilolite (clin) and kaolin were chosen for grafting SO_3H- group, and tested their performance on cyclopentanone condensation. The acid–base density and intensity of the catalysts were determined using CO_2-TPD and NH_3-TPD measurements, and the results were shown in Figure 2c,d. The CO_2 desorption curve showed that there was a diffraction peak below 150 °C which could be attributed to the weakly basic centers, and the diffraction peak in the range of 150–450 °C which could be attributed to the medium sites. The ammonia desorption curve existed an acidic desorption site at approximately 450 °C, which was assumed to be the strong acidity of the sulfonic acid group (-SO_3H) [39]. The results of the quantitative analysis of CO_2-TPD and NH_3-TPD data were shown in Table 1, which indicated that the SO_3H-APG catalyst possessed both acid–base properties, with its basic sites mainly concentrated in the medium-base position. Additionally, it also reflected that the acid–base bifunctional catalyst could promote the cyclopentanone condensation reaction efficiently.
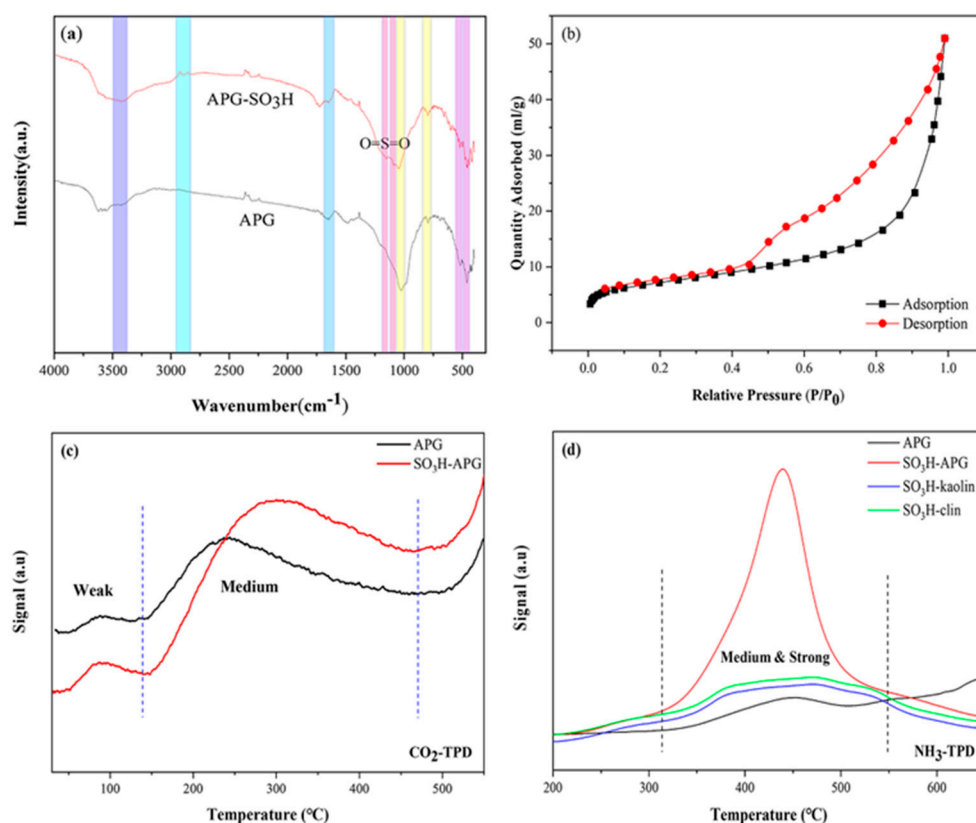
Figure 2. The (**a**) FT-IR, (**b**) N$_2$ adsorption–desorption isotherms, (**c**) CO$_2$-TPD, and (**d**) NH$_3$-TPD spectra of clay-based catalysts.

Table 1. Physiochemical properties of catalysts.

	CO$_2$ Quantity (cm^3/g)		Base Amount (mmol/g)			NH$_3$ Quantity (cm^3/g)	Total Acids (mmol/g)
	0–150 °C	150–450 °C	Weak Base	Medium Base	Total Basicity		
APG	39.76	85.31	1.81	3.88	5.69	17.63	1.04
SO$_3$H-APG	34.67	83.81	1.58	3.81	5.39	99.60	5.86
SO$_3$H-kaolin	-	-	-	-	-	28.39	1.67
SO$_3$H-clin	-	-	-	-	-	31.78	1.87

The TPD curves were fitted with split peaks, and both Yang [40] and Hu [41,42] methods were used to calculate the activation energy of desorption (DAE) for the acidic and basic sites (Table S4). It can be seen that the desorption temperatures (thermos-desorption temperatures of CO$_2$ and NH$_3$ are related to basicity and acidity strength, respectively) corresponding to the medium base site desorption peaks of APG and SO$_3$H-APG catalysts were 236.14 °C and 295.04 °C, and the corresponding E_d values calculated by Hu are 36.29 kJ/mol and 44.11 kJ/mol, respectively. Meanwhile, the desorption temperature corresponding to the medium-strong acid sites desorption peak of SO$_3$H-APG catalyst was 438.93 °C, and the activation energy of resolution calculated by Yang's method was 23.72 kJ/mol. The adsorption performance of the adsorbent depended not only on its porous structure but also on the chemical properties of its surface [43]. the stronger the adsorption of the adsorbent with the catalyst's surface was, and the more difficult for desorption [44]. The above results indicated that the SO$_3$H-APG catalyst with a strong medium base and acidic sites played an important role in facilitating the catalytic conversion of cyclopentanone.

The surface areas and pore volumes of these three catalysts were listed in Table 2. Typical mesoporous structure remained when the sulfonic acid groups were grafted, which may point to a few amounts of pore blockage.

Table 2. Physical properties of SO$_3$H-APG, SO$_3$H-kaolin, and SO$_3$H-clin catalyst.

	BET Surface Area (m^2/g)	Pore Volume (cm^3/g)	Pore Diameter (nm)
SO$_3$H-APG	127.08	0.0312	0.95 (micro)/3.83 (meso)
SO$_3$H-kaolin	117.04	0.1399	3.84
SO$_3$H-clin	110.94	0.2639	3.82

2.2. Screening of Reaction Conditions

The effects of different reaction parameters on the cyclopentanone conversion and the selectivity of the condensation products (C10, C15) with SO$_3$H-APG as the catalyst were shown in Figure 3. It can be seen that the conversion of cyclopentanone without the introduction of sulfonic acid groups was 53.21 ± 2.66%, and the yield and selectivity of the target product (dimer and trimer) reached 35.85 ± 1.79% and 67.46 ± 3.37% Figure 3a. The highest conversion of cyclopentanone (79.96 ± 3.99%) was achieved at the -SO$_3$H loading of 4 mmol/g, and the total yield and selectivity of its condensation products also reached the maximum values of 68.01 ± 3.40% and 85.05 ± 4.25%, respectively. As the loading of sulfonic acid groups continued to increase, the conversion and the selectivity of the condensate decreased, which may be because the excess of -SO$_3$H groups covered part of the active sites on the catalyst, reducing its specific surface area, pore volume as well as the catalytic activity [45]. Natural clay minerals contain basic sites such as MgO and Al$_2$O$_3$, and the introduction of acidic sites can achieve acid–base synergistic catalysis and, therefore, promote cyclopentanone condensation.

The influence of reaction temperature on the condensation performance was investigated in the range of 110–170 °C, as shown in Figure 3b. At the condensation temperature of 150 °C, the conversion of cyclopentanone reached the maximum of 85.53 ± 1.28%, and the yield of the target product was approximately 83.35 ± 4.03% (dimer, 59.05 ± 2.95%; trimer, 24.3 ± 1.08%). However, when the temperature was further increased to 170 °C, the conversion and yield decreased significantly, so 150 °C was selected as the optimized condensation temperature. The selectivity of the dimer and trimer as a function of condensation temperature was shown in Figure 3(b2). With the increase of condensation temperature, the selectivity to the trimer inclined clearly, and the dimer selectivity reached more than 60%. In the production of jet fuel intermediates from furfural and acetone, a similar conclusion was drawn by Huang et al. It was found that higher temperature might promote the degradation of the F$_3$A$_2$ intermediate, thus, improving the selectivity of aldol condensation products [46].

The effect of different reaction times on the condensation performance of cyclopentanone was displayed in Figure 3c. The conversion enhanced obviously with the increase in reaction time at the early stage of the reaction, and reached quickly 80.23 ± 2.40% at 4 h. At this time, the yield and selectivity of the condensation products (dimer and trimer) were 69.81 ± 2.43% and 87.02 ± 4.35%. When the reaction time was extended, the conversion of cyclopentanone remained stable, so the optimal reaction time was chosen to be 4 h.

The influence of the different catalysts on the cyclopentanone conversion and product selectivity were shown in Figure 3d. It was seen that SO$_3$H-APG exhibited a superior catalytic effect in the cyclopentanone condensation reaction compared to SO$_3$H-kaolin and SO$_3$H-clin catalysts. The conversion of cyclopentanone reached 85.53 ± 0.85%, meanwhile, the selectivity of the target products (Figure S1) also attained the highest (dimer, 69.04 ± 3.45%; trimer, 28.41 ± 1.42%). Moreover, tt indicated that the acid–base synergism promoted the efficient condensation of cyclopentanone.
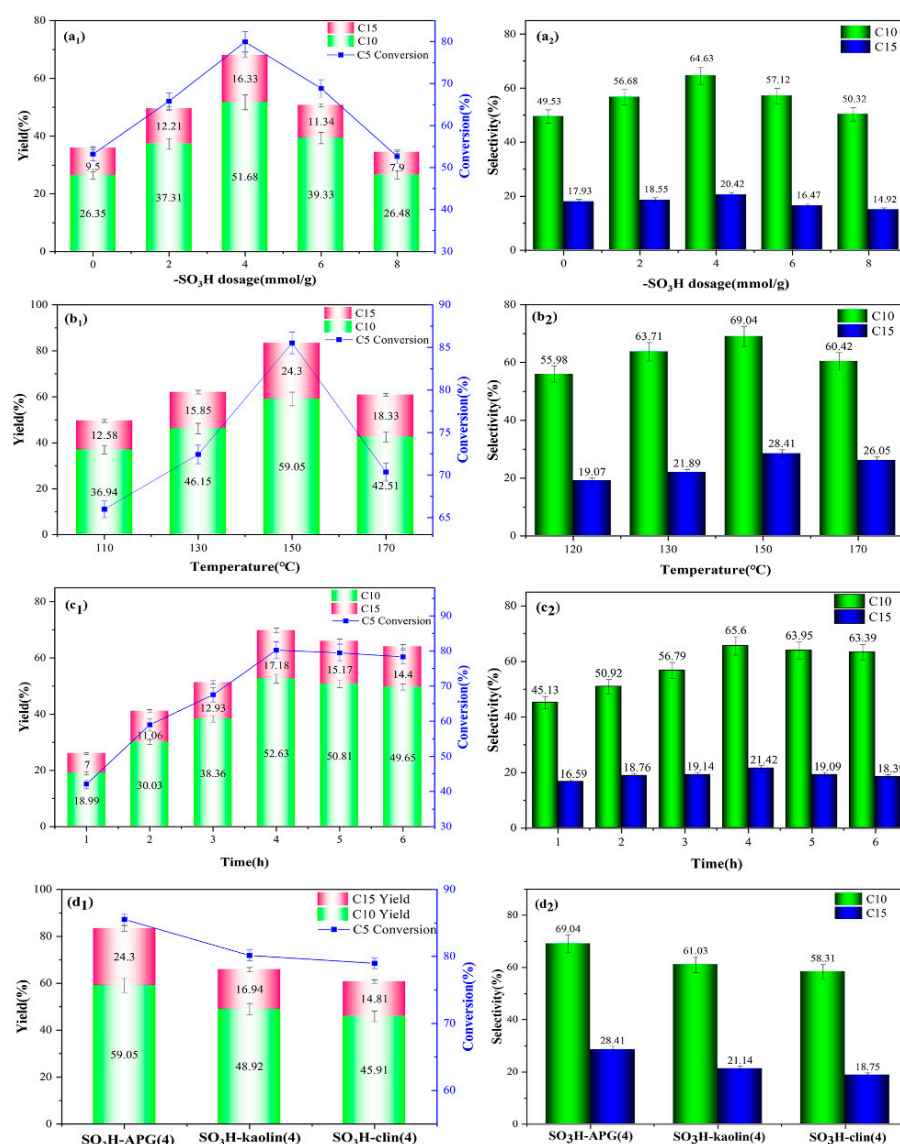
Figure 3. Effect of (**a**) -SO$_3$H loading, 150 °C, 4 h; (**b**) reaction temperature, 4 mmol/g, 4 h; (**c**) reaction time, 150 °C, 4 mmol/g; (**d**) catalyst on the condensation reaction of cyclopentanone. Reaction conditions: 0.6 g catalyst, 4 g cyclopentanone, 200 rpm. Letter+1 for yield and letter+2 for selectivity.

2.3. Response Surface Methodology (RSM) Analysis

Based on the single-factor experiment, the C10 yield was taken as the response value, and the three factors that had a significant effect on the cyclopentanone condensation reaction, -SH loading (X1), reaction temperature (X2) and reaction time (X3), were investigated and analyzed according to the Box–Behnken principle using Design expert V8.0.6 software (Table S2). The response results of the interaction among the factors were shown in Figure 4.

From the analysis, it can be seen that when the -SH loading, and reaction time were unchanged. The yield of C10 showed a trend of increasing and then decreasing with the heightened reaction temperature in response to the sensitivity. When the reaction temperature and -SH loading was fixed, the yield of C10 also showed a tendency to raise and then reduce with the protracted reaction time, which had a large effect. The reaction time and reaction temperature were fixed, and the yield of C10 showed the same trend and corresponding sensitivity as the loading of sulfhydryl groups increased. The contours were closed elliptical and the response surface was convexed, indicating a strong interaction between the factors and a maximum.

The results were analyzed by stepwise regression using the software (Tables S2 and S3), and the optimal reaction conditions were determined as -SH loading 1.65 mL, reaction temperature 150.81 °C, and reaction time 4.11 h. At this time, the yield of C10 was 59.02%. To facilitate the practical operation, the optimal reaction conditions were revised to -SH loading 1.6 mL, reaction temperature 150 °C, and reaction time 4 h. The yield of C10 reached 59.05% under these optimal conditions, which was in good agreement with the predicted value of the model and verified the reliability of the approach.
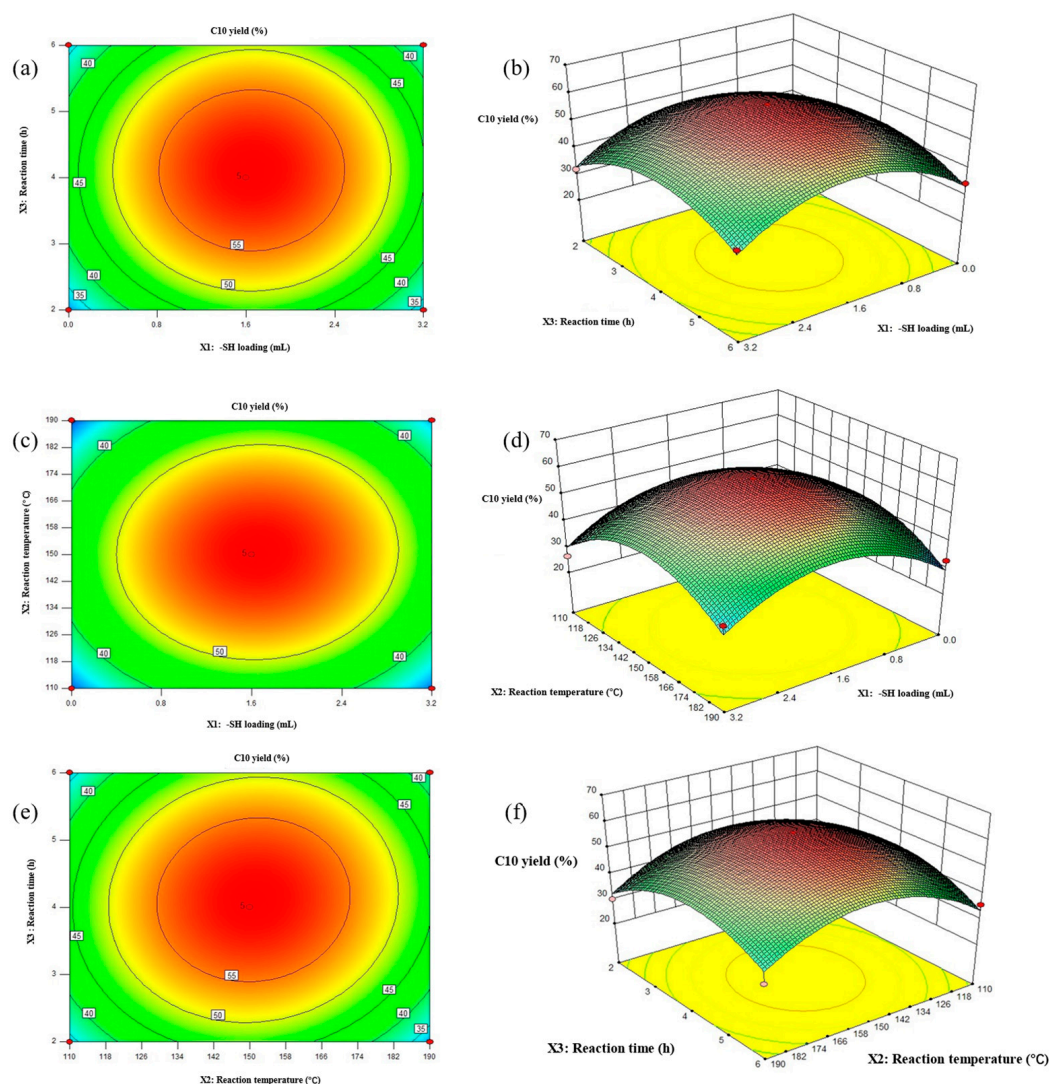
Figure 4. Response surface analysis of C10 yield in a cyclopentanone condensation reaction. Contour plot of C10 yield: (**a**) -SH loading and reaction time; (**c**) -SH loading and reaction temperature; (**e**) Reaction temperature and reaction time; Response surface diagram: (**b**) -SH loading and reaction time; (**d**) -SH loading and reaction temperature; (**f**) Reaction temperature and reaction time.

2.4. Reaction Kinetic Analysis

To investigate the operating reaction mechanisms of the acid–base bifunctional catalyst, the variations of cyclopentanone concentration as the change of time on the different catalysts were measured under water-free conditions. When the surface coverage was low enough to vary with reactant concentration, the intrinsic reaction order could be better individualized at low reactant concentrations [47]. In addition to obtaining kinetic expressions useful for the calculation of activation energy, the kinetic model for the catalytic and non-catalytic conversion of cyclopentanone also provided a clearer knowledge of how the conversion process at the catalysts works. The graphs of $\ln(C_0/C)$ against

time gave good straight-line plots, and this revealed that the cyclopentanone aldol condensation reaction followed first-order kinetics Figure 5a. Based on this, we fitted the typical Langmuir-Hinshelwood (L-H) model, and the results showed that the R^2 was all greater than 0.95 Figure 5b, indicating a strong fit, and the detailed derivation process was described in the supplementary material.
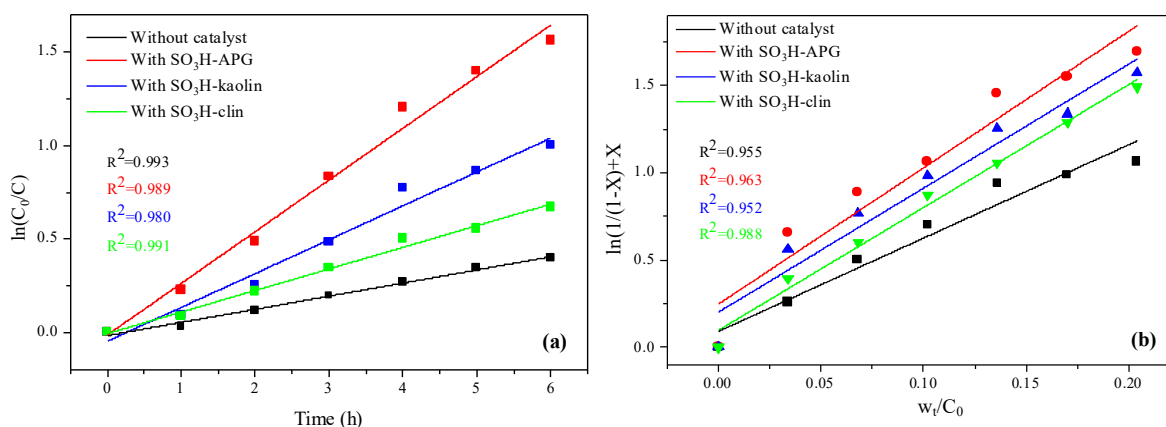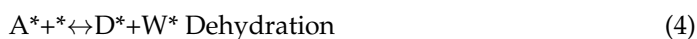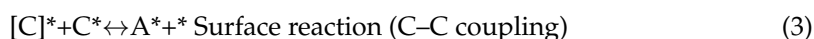

Figure 5. (**a**) First-order kinetic, (**b**) Langmuir–Hinshelwood (L-H) kinetics model fitted for cyclopentanone aldol condensation at different catalysts.

The basic steps of the catalytic cyclopentanone via aldol condensation mainly included the adsorption of cyclopentanone, the formation of enol, C–C coupling, dehydration and product desorption [48–50], and the detailed mechanism was shown in Equations (1)–(6), where C represented the reactant cyclopentanone, * stood for the available surface active sites, A was the alcohol product, D was the dimer product (C10), and W was water. The attack of the enol on the electrophilic carbon of the other carbonyl group was the rate-limiting step of the reaction [47], which means that the C–C coupling had a certain limiting effect on the cyclopentanone self-condensation.

$$C+* \leftrightarrow C* \text{ Adsorption of cyclopentanone} \tag{1}$$

$$C* \leftrightarrow [C]* \text{ Formation of enol} \tag{2}$$

$$[C]*+C* \leftrightarrow A*+* \text{ Surface reaction (C–C coupling)} \tag{3}$$

$$A*+* \leftrightarrow D*+W* \text{ Dehydration} \tag{4}$$

$$D* \leftrightarrow D+* \text{ Desorption of dimer} \tag{5}$$

$$W* \leftrightarrow W+* \text{ Desorption of water} \tag{6}$$

2.5. The Mechanism of Acid–Base Bifunctional Catalyst Action

Given that the SO_3H-APG catalyst showed high catalytic activity in the cyclopentanone aldol condensation reaction, it is evident that the acid and base centers have an important role in this reaction, and therefore the reaction mechanism of the acid–base bifunctional catalyst in this condensation reaction was investigated. APG is a mineral aluminosilicate with about 2:1 (mol ratio) Mg to Al in its framework, which made it has abundant accessible base sites and active for base-catalytic condensation. Trace amount of Fe, Ni cations in APG would promote H_2O adsorption and dissociation. As shown in Figure 6, the α-H on the carbonyl oxygen atom side of the cyclopentanone was deprotonated by the catalytic action of the basic site on the SO_3H-APG catalyst to form a carbon-negative ion, which was then added to the carbonyl carbon atom of another cyclopentanone molecule to form a β-hydroxy aldehyde after deprotonation. Finally, the dimer was prepared by dehydration under heating conditions using hydroxy aldehyde as the raw material. The α-H on the other side reacted with the carbonyl carbon atom of another cyclopentanone molecule

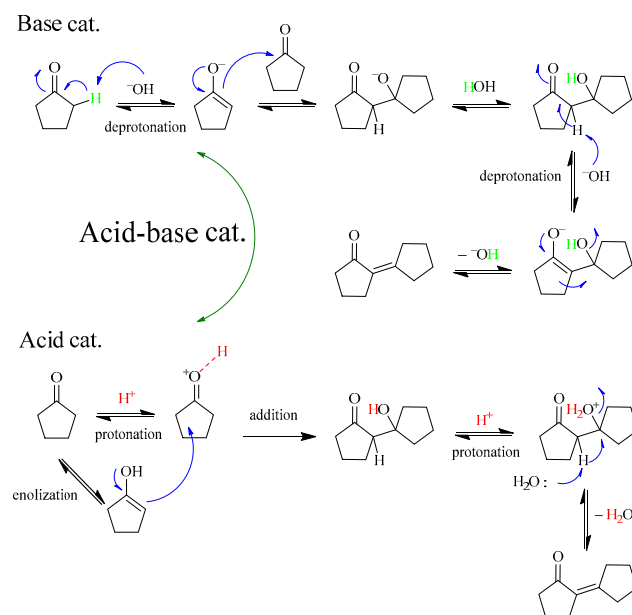in the nucleophilic addition reaction, and after dehydration, the target product (trimer) was formed.

Figure 6. Reaction routes of cyclopentanone condensation reaction on the acid–base bifunctional catalyst. (OH^- presented catalytic base site on SO_3H-APG).

Under the catalytic effect of the acidic sites, the enolized structure of cyclopentanone and the carbon-positive ion structure proceeds to an addition reaction. Followed by dehydration to form an enone structure, which was unstable, and the electron cloud was shifted toward the hydroxyl group to form a carbon-positive ion after protonation, and the carbon-positive ion was dehydrogenated to form a stable dimer. Accordingly, the acid–base sites cooperated to promote the continuity of the cyclopentanone condensation reaction, which was also consistent with the analytical results of CO_2-TPD as well as NH_3-TPD. Additionally, it was indicated as an exothermal adsorption of cyclopentanone. Increasing in the adsorbate electron density will facilitate its activation and further condensation (Figure S5).

As for the mechanism that was proposed by the Wang group [51] for efficient C–C coupling of acetone by separated dual sites, carbocation derived on the acid site was combined with carbanion on the base site at a reasonably high rate ($1020 \text{ mg} \cdot g_{CAT}^{-1} \cdot h^{-1}$). The enhanced cyclopentanone yield on the SO_3H-APG catalyst can illustrate the promotion effect of the ion pair (positive-negative) interaction on spatially isolated acid and base sites that worked synergistically.

2.6. Catalyst Stability and Recycling

These mineral-based catalysts were easily recycled at the end of the reaction and could be recycled after filtering, washing, and drying. The changes during the conversion of cyclopentanone and the C10 and C15 selectivity of the SO_3H-APG catalyst after five cycles were demonstrated in Figure 7a. As can be seen from the figure, the overall conversion and selectivity of the catalysts remained stable with the increase in the number of cycles, and the reduced activity may be caused by the deactivation of some active centers of the catalysts.

To explore the reusability of the catalyst, the catalyst after recycling for five times was subjected to FT-IR analysis, and the results were shown in Figure 7b. The results showed that the FT-IR spectra of the recycled SO_3H-APG catalyst revealed bands that were similar to the fresh catalyst, indicating that the catalyst was stable and still had a significant amount of acid–base centers after participating in the reaction.
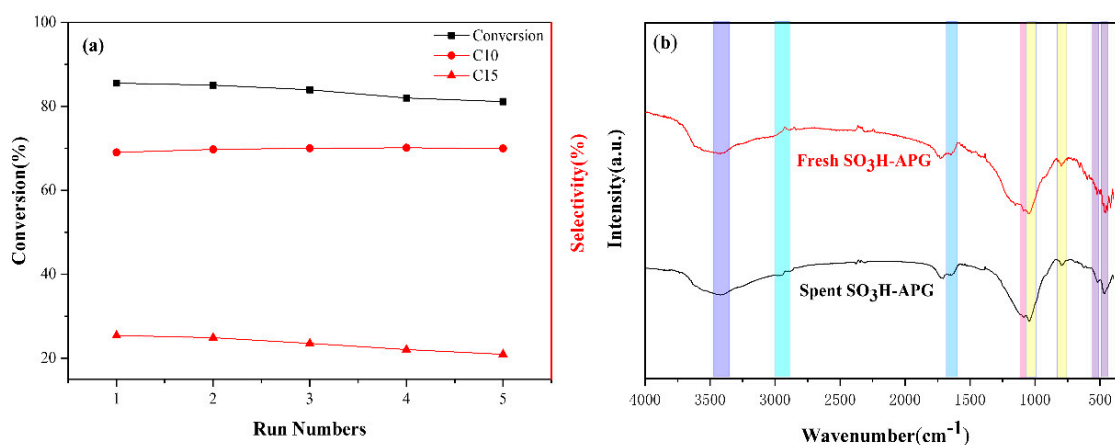
Figure 7. Recycling performance of SO$_3$H-APG catalyst. (**a**) Catalytic performance. (**b**) FT-IR spectra of fresh and 5-run spent catalysts.

3. Materials and Method

3.1. Materials and Equipment

APG, SiO$_2$ (purity 85-90%) were purchased from Changzhou DingBang Mineral Products Technology, Huaian, China. 3-mercaptopropyl trimethoxysilane (MPTMS, purity 95%) were purchased from Aladdin Reagent (Shanghai) Co., Ltd., Shanghai, China. H$_2$O$_2$ were purchased from Sinopharm Chemical Reagent Co., Ltd., Shanghai, China. Ball mill was purchased from Zhuo's Instrument Co., Ltd., Shanghai, China. All chemicals were used without further purification.

3.2. Preparation of SO$_3$H-APG Catalyst

The synthesis of the SO$_3$H-APG catalyst was derived from a previous study [52]. Firstly, 2 g attapulgite, 1.6 mL 3-mercaptopropyl trimethoxysilane (MPTMS, 95%), 10 mL water were added to a 50 mL resin tank (containing agate medium pellets of 5–9 mm in diameter), and reacted using a planetary ball mill at 300 rpm for 2.5 h to obtain the APG-SH. Then, the prepared APG-SH was functioned by consecutive H$_2$O$_2$ (30 wt%) oxidation (stirred at room temperature for 12 h), washed with distilled water after oxidation, and dried at 80 °C to obtain the SO$_3$H-APG catalyst (Figure 8).
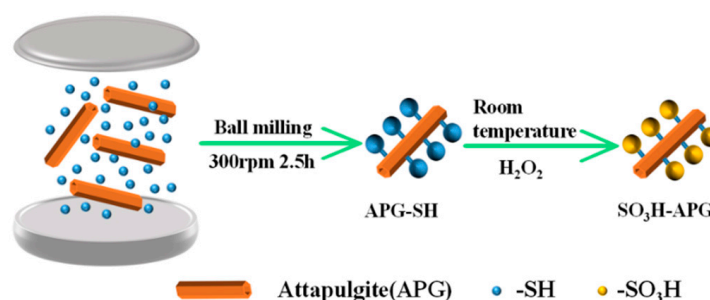

Figure 8. Preparation route of SO$_3$H-APG catalyst.

Other natural aluminosilicates, kaolin, and clinoptilolite (clin) are also abundant mineral clays that have porous structures and acid sites that are benign for cyclopentanone condensation. Which made them the references of APG clay. SO$_3$H-kaolin and SO$_3$H-clin samples were synthesized following a similar procedure of SO$_3$H-APG preparation for reference.

3.3. Catalyst Characterization

The FT-IR spectra of the catalysts were recorded on Nicolet 6700 (Thermo Electron Corporation, Waltham, MA, USA) in the range from 400 to 4000 cm^{-1}. The N$_2$ adsorption–

desorption isotherms were collected with a BSD-PM2 instrument, and the pore size distribution curves were determined using the NLDFT mathematical model. The high-resolution morphology was observed under the SEM microscope (Gemini SEM 300, ZEISS, Jena, Germany) and TEM microscope (JEM-2100, JEOL Ltd., Tokyo, Japan) to characterize the catalyst. The temperature-programmed desorption tests, NH_3-TPD and CO_2-TPD, were performed with AutoChem II 2920 (Micromeritics Instrument Corp., Norcross, GA, USA). Catalyst samples were pretreated at He (300 °C, 60 min) and exposed to ammonia at 200 °C until saturation and then stopped heating. After the chamber was cooled down to room temperature, the NH_3-TPD experiments were performed between 50 °C and 700 °C with a desorption rate of 10 °C/min. The CO_2-TPD process was carried out in the same way, with the catalyst adsorbed to saturation with CO_2.

3.4. Aldol Condensation of Cyclopentanone

The aldol condensation reaction of cyclopentanone (analytic purity) was carried out on a digital thermostatic heating sleeve with magnetic stirring. Under solvent-free conditions, a quantitative amount of catalyst and cyclopentanone (catalyst/cyclopentanone mass ratio, 0.15) were added to a round-bottom 100 mL glass flask and mixed well. The electric heating sleeve was preheated to the specified temperature and then stirred at 200 rpm under reflux. After the reaction, the flask was cooled to room temperature, and the condensation samples were transferred and processed in a high-speed centrifuge. The liquid products were diluted with CH_2Cl_2 (chromatographic purity) into the volumetric flask for analysis, and repeated experiments were conducted after the solid catalyst was washed and dried.

Using Design expert V8.0.6 software to fit the data in Table S2, the regression equation S1 was obtained. Analysis of variance was performed on the above regression equation and the results are tabulated in Table S3.

Filtration was used to recover post-reaction catalysts, which were then cleaned with ethanol under ultrasonic conditions for 1h and dried overnight before being reused.

3.5. Products Analysis

The reaction products were analyzed by gas chromatography-mass spectrometry (GC-MS, Agilent 7890-5975C, Santa Clara, CA, USA), equipped with an Agilent 7683B auto-injector, an HP-5 capillary column and a Flame Ionization Detector (FID), and gas chromatography (Agilent 6890, HP-5 capillary column, 30.0 m × 250 mm × 0.25 mm) was used for quantitative analysis. The conversion of cyclopentanone, the selectivity of C10, and the yield were calculated according to the following Equations (7)–(9).

$$\text{Conversion} = (1 - \frac{\text{Moles of cyclopentanone}}{\text{Moles of cyclopentanone loaded initially}}) \times 100\% \tag{7}$$

$$\text{Selectivity of C10} = \frac{\text{Moles of cyclopentanone to C10}}{\text{Moles of cyclopentanone converted}} \times 100\% \tag{8}$$

$$\text{Yield of C10} = \text{selectivity} \times \text{conversion} \tag{9}$$

4. Conclusions

A variety of mineral-based catalysts were synthesized by a simple and eco-friendly milling method and used in the cyclopentanone aldol condensation reaction under solvent-free conditions. Among them, the SO_3H-APG catalysts with large specific surfaces and abundant acid–base sites showed good catalytic effects. The optimization of the reaction conditions and the response surface analysis revealed that the conversion of cyclopentanone reached a maximum of 85.53% when the $-SO_3H$ loading of 4 mmol/g, reaction temperature of 150 °C, and reaction time of 4 h. The selectivity and yield of the dimer and trimer were also maximized at 69.04% and 28.41%, respectively. In addition, the SO_3H-APG catalyst has shown excellent stability in long-term reaction and recycling runs.

References

1. Choe, B.; Lee, S.; Won, W. Process integration and optimization for economical production of commodity chemicals from lignocellulosic biomass. *Renew. Energy* **2020**, *162*, 242–248. [CrossRef]
2. Huchede, M.; Lorentz, C.; Cardenas, L.; Morvan, D.; Belliere-Baca, V.; Millet, J.M.M. Gas phase dehydration of 3-hydroxybutanone on orthophosphate catalysts for bio-based production of butenone for a sustainable industrial route to vitamin A. *J. Ind. Eng. Chem.* **2020**, *88*, 178–185. [CrossRef]
3. Jiang, Y.; Liu, H.; Zhao, H.; Zhou, R.; Du, W.; Wang, S.; Hou, Z. Synthesis of 3-hydroxybutyraldehyde over highly stable solid base catalysts prepared from layered double hydroxides. *Appl. Clay Sci.* **2021**, *214*, 106277. [CrossRef]
4. Niu, Y.; Lv, Y.; Lei, Y.; Liu, S.; Liang, Y.; Wang, D.; Hui, S.e. Biomass torrefaction: Properties, applications, challenges, and economy. *Renew. Sustain. Energy Rev.* **2019**, *115*, 109395. [CrossRef]
5. Phromphithak, S.; Meepowpan, P.; Shimpalee, S.; Tippayawong, N. Transesterification of palm oil into biodiesel using ChOH ionic liquid in a microwave heated continuous flow reactor. *Renew. Energy* **2020**, *154*, 925–936. [CrossRef]
6. Tempelman, C.H.L.; Jacobs, J.F.; Ramkhelawan, S.; Mok, A.; van der Zalm, W.; Degirmenci, V. Processing of agricultural apple fruit waste into sugar rich feedstocks for the catalytic production of 5-HMF over a Sn Amberlyst-15 resin catalyst. *J. Ind. Eng. Chem.* **2021**, *99*, 443–448. [CrossRef]
7. Hita, I.; Cordero-Lanzac, T.; Bonura, G.; Cannilla, C.; Arandes, J.M.; Frusteri, F.; Bilbao, J. Hydrodeoxygenation of raw bio-oil towards platform chemicals over FeMoP/zeolite catalysts. *J. Ind. Eng. Chem.* **2019**, *80*, 392–400. [CrossRef]
8. Jing, Y.; Xin, Y.; Guo, Y.; Liu, X.; Wang, Y. Highly efficient Nb_2O_5 catalyst for aldol condensation of biomass-derived carbonyl molecules to fuel precursors. *Chin. J. Catal.* **2019**, *40*, 1168–1177. [CrossRef]
9. Shao, S.; Dong, W.; Li, X.; Zhang, H.; Xiao, R.; Cai, Y. Solvent-free synthesis of jet fuel by aldol condensation and hydroprocessing of cyclopentanone as biomass-derivates. *J. Clean. Prod.* **2020**, *250*, 119459. [CrossRef]
10. Sheng, X.; Xu, Q.; Wang, X.; Li, N.; Jia, H.; Shi, H.; Niu, M.; Zhang, J.; Ping, Q. Waste Seashells as a Highly Active Catalyst for Cyclopentanone Self-Aldol Condensation. *Catalysts* **2019**, *9*, 661. [CrossRef]
11. Yan, L.; Zhang, J.; Gao, X.; Song, F.; Wang, X.; Zhang, T.; Liu, X.; Meng, X.; Zhang, Q.; Han, Y.; et al. Oxidative coupling of methane over Mo-Sn catalysts. *Chem. Commun.* **2021**, *57*, 13297–13300. [CrossRef] [PubMed]
12. Yan, L.; Zhang, J.-L.; Hu, H.-M.; Wang, F.; Bai, C.; Li, X.-Y.; Wang, X.; Wang, B.-Z. Structural diversity and near-infrared luminescence of lanthanide coordination polymers with different flexibility and coordination orientation based on bipyridyl carboxylate and dicarboxylate ligands. *J. Solid State Chem.* **2020**, *292*, 121654. [CrossRef]
13. Kunkes, E.L.; Simonetti, D.A.; West, R.M.; Serrano-Ruiz, J.C.; Gartner, C.A.; Dumesic, J.A. Catalytic conversion of biomass to monofunctional hydrocarbons and targeted liquid-fuel classes. *Science* **2008**, *322*, 417–421. [CrossRef] [PubMed]
14. Zhang, X.; Lei, H.; Zhu, L.; Wu, J.; Chen, S. From lignocellulosic biomass to renewable cycloalkanes for jet fuels. *Green Chem.* **2015**, *17*, 4736–4747. [CrossRef]
15. Bano, K.; Jain, A.; Sarkar, R.; Panda, T.K. Economically Viable and Efficient Catalysts for Esterification and Cross Aldol Condensation Reactions under Mild Conditions. *Chemistryselect* **2020**, *5*, 4470–4477. [CrossRef]
16. Deng, Q.; Nie, G.; Pan, L.; Zou, J.-J.; Zhang, X.; Wang, L. Highly selective self-condensation of cyclic ketones using MOF-encapsulating phosphotungstic acid for renewable high-density fuel. *Green Chem.* **2015**, *17*, 4473–4481. [CrossRef]
17. Han, P.; Nie, G.; Xie, J.; E, X.-T.-F.; Pan, L.; Zhang, X.; Zou, J.-J. Synthesis of high-density biofuel with excellent low-temperature properties from lignocellulose-derived feedstock. *Fuel Process. Technol.* **2017**, *163*, 45–50. [CrossRef]
18. Wang, H.; Wang, Z.; Wang, S.; Yang, C.; Li, S.; Gao, P.; Sun, Y. The effect of the particle size on Fischer-Tropsch synthesis for ZSM-5 zeolite supported cobalt-based catalysts. *Chem. Commun.* **2021**, *57*, 13522–13525. [CrossRef]
19. Cui, X.; Zhao, X.; Liu, D. A novel route for the flexible preparation of hydrocarbon jet fuels from biomass-based platform chemicals: A case of using furfural and 2,3-butanediol as feedstocks. *Green Chem.* **2018**, *20*, 2018–2026. [CrossRef]

20. Veloso, C.O.; Perez, C.N.; de Souza, B.M.; Lima, E.C.; Dias, A.G.; Monteiro, J.L.F.; Henriques, C.A. Condensation of glyceraldehyde over Mg,Al-mixed oxides derived from hydrotalcites. *Microporous Mesoporous Mater.* **2008**, *107*, 23–30. [CrossRef]

21. Collier, V.E.; Ellebracht, N.C.; Lindy, G.I.; Moschetta, E.G.; Jones, C.W. Kinetic and Mechanistic Examination of Acid-Base Bifunctional Aminosilica Catalysts in Aldol and Nitroaldol Condensations. *ACS Catal.* **2016**, *6*, 460–468. [CrossRef]

22. Faba, L.; Diaz, E.; Ordonez, S. Hydrodeoxygenation of acetone-furfural condensation adducts over alumina-supported noble metal catalysts. *Appl. Catal. B-Environ.* **2014**, *160*, 436–444. [CrossRef]

23. Hronec, M.; Fulajtarova, K.; Liptaj, T.; Stolcova, M.; Pronayova, N.; Sotak, T. Cyclopentanone: A raw material for production of C-15 and C-17 fuel precursors. *Biomass Bioenergy* **2014**, *63*, 291–299. [CrossRef]

24. Cueto, J.; Faba, L.; Diaz, E.; Ordonez, S. Cyclopentanone as an Alternative Linking Reactant for Heterogeneously Catalyzed Furfural Aldol Condensation. *Chemcatchem* **2017**, *9*, 1765–1770. [CrossRef]

25. Huang, R.; Chang, J.; Choi, H.; Vohs, J.M.; Gorte, R.J. Furfural Upgrading by Aldol Condensation with Ketones over Solid-Base Catalysts. *Catal. Lett.* **2022**, *152*, 3833–3842. [CrossRef]

26. de Reviere, A.; Gunst, D.; Sabbe, M.; Verberckmoes, A. Sustainable short-chain olefin production through simultaneous dehydration of mixtures of 1-butanol and ethanol over HZSM-5 and gamma-Al₂O₃. *J. Ind. Eng. Chem.* **2020**, *89*, 257–272. [CrossRef]

27. Diaz-Sanchez, M.; Gomez, I.J.; Prashar, S.; Horacek, M.; Lamac, M.; Urban, B.; Pinkas, J.; Gomez-Ruiz, S. Multifunctional catalysts based on palladium nanoparticles supported on functionalized halloysites: Applications in catalytic C-C coupling, selective oxidation and dehalogenation reactions. *Appl. Clay Sci.* **2021**, *214*, 106272. [CrossRef]

28. Sudarsanam, P.; Peeters, E.; Makshina, E.V.; Parvulescu, V.I.; Sels, B.F. Advances in porous and nanoscale catalysts for viable biomass conversion. *Chem. Soc. Rev.* **2019**, *48*, 2366–2421. [CrossRef] [PubMed]

29. Vaculikova, L.; Valovicova, V.; Plevova, A.E.; Napruszewska, B.D.; Duraczynska, D.; Karcz, R.; Serwicka, E.M. Synthesis, characterization and catalytic activity of cryptomelane/montmorillonite composites. *Appl. Clay Sci.* **2021**, *202*, 105977. [CrossRef]

30. Shao, S.; Hu, X.; Dong, W.; Li, X.; Zhang, H.; Xiao, R.; Cai, Y. Integrated C-C coupling/hydrogenation of ketones derived from biomass pyrolysis for aviation fuel over Ni/Mg-Al-O/AC bifunctional catalysts. *J. Clean. Prod.* **2021**, *282*, 124331. [CrossRef]

31. Zeidan, R.K.; Davis, M.E. The effect of acid-base pairing on catalysis: An efficient acid-base functionalized catalyst for aldol condensation. *J. Catal.* **2007**, *247*, 379–382. [CrossRef]

32. Zhao, X.; Li, S.; Hu, Y.; Zhang, X.; Chen, L.; Wang, C.; Ma, L.; Zhang, Q. Synthesis of long chain alkanes via aldol condensation over modified chitosan catalyst and subsequent hydrodeoxygenation. *Chem. Eng. J.* **2022**, *428*, 131368. [CrossRef]

33. Amarasekara, A.S.; Wiredu, B.; Grady, T.L.; Obregon, R.G.; Margetic, D. Solid acid catalyzed aldol dimerization of levulinic acid for the preparation of C10 renewable fuel and chemical feedstocks. *Catal. Commun.* **2019**, *124*, 6–11. [CrossRef]

34. Paniagua, M.; Cuevas, F.; Morales, G.; Melero, J.A. Sulfonic Mesostructured SBA-15 Silicas for the Solvent-Free Production of Bio-Jet Fuel Precursors via Aldol Dimerization of Levulinic Acid. *ACS Sustain. Chem. Eng.* **2021**, *9*, 5952–5962. [CrossRef]

35. Albach, B.; Liz, M.V.; Prola, L.D.T.; Barbosa, R.V.; Campos, R.B.; Rampon, D.S. Eco-friendly mechanochemical intercalation of imidazole into kaolinite. *J. Solid State Chem.* **2020**, *292*, 121649. [CrossRef]

36. Murtaza, S.Z.M.; Vaqueiro, P. Rapid synthesis of chalcohalides by ball milling: Preparation and characterisation of BiSI and BiSeI. *J. Solid State Chem.* **2020**, *291*, 121625. [CrossRef]

37. Li, X.; Zhang, J.; Liu, B.; Liu, J.; Wang, C.; Chen, G. Hydrodeoxygenation of lignin-derived phenols to produce hydrocarbons over Ni/Al-SBA-15 prepared with different impregnants. *Fuel* **2019**, *243*, 314–321. [CrossRef]

38. Xing, R.; Liu, N.; Liu, Y.; Wu, H.; Jiang, Y.; Chen, L.; He, M.; Wu, P. Novel solid acid catalysts: Sulfonic acid group-functionalized mesostructured polymers. *Adv. Funct. Mater.* **2007**, *17*, 2455–2461. [CrossRef]

39. Thi Tuong Vi, T.; Kongparakul, S.; Karnjanakom, S.; Reubroycharoen, P.; Guan, G.; Chanlek, N.; Samart, C. Highly productive xylose dehydration using a sulfonic acid functionalized KIT-6 catalyst. *Fuel* **2019**, *236*, 1156–1163. [CrossRef]

40. Yang, D.H.; Hur, B.Y.; He, D.P.; Yang, S.R. Effect of decomposition properties of titanium hydride on the foaming process and pore structures of Al alloy melt foam. *Mater. Sci. Eng. A-Struct. Mater. Prop. Microstruct. Process.* **2007**, *445*, 415–426. [CrossRef]

41. Ellison, C.; Hoffman, J.; Shekhawat, D. Comparison of microwave and conventional heating for CO₂ desorption from zeolite 13X. *Int. J. Greenh. Gas Control* **2021**, *107*, 103311. [CrossRef]

42. Yu, C.; Qi, Z.; Bian, J.; Song, R.; Wang, W.; Li, C. Insight into acid-base bifunctional catalysts for microalgae liquefaction and bio-oil pyrolysis: Product characteristics, energy recovery and kinetics. *J. Anal. Appl. Pyrolysis* **2021**, *155*, 105086. [CrossRef]

43. Zhang, K.; Cheung, W.H.; Valix, M. Roles of physical and chemical properties of activated carbon in the adsorption of lead ions. *Chemosphere* **2005**, *60*, 1129–1140. [CrossRef] [PubMed]

44. Xia, Q.; Li, Z.; Xiao, L.; Zhang, Z.; Xi, H. Effects of loading different metal ions on an activated carbon on the desorption activation energy of dichloromethane/trichloromethane. *J. Hazard. Mater.* **2010**, *179*, 790–794. [CrossRef]

45. Xue, B.; Li, Y.; Deng, L. Selective synthesis of p-xylene by alkylation of toluene with dimethyl carbonate over MgO-modified MCM-22. *Catal. Commun.* **2009**, *10*, 1609–1614. [CrossRef]

46. Huang, X.; Zhang, Q.; Wang, T.; Liu, Q.; Ma, L.; Zhang, Q. Production of jet fuel intermediates from furfural and acetone by aldol condensation over MgO/NaY. *J. Fuel Chem. Technol.* **2012**, *40*, 973–978. [CrossRef]

47. Li, G.; Wang, B.; Chen, B.; Resasco, D.E. Role of water in cyclopentanone self-condensation reaction catalyzed by MCM-41 functionalized with sulfonic acid groups. *J. Catal.* **2019**, *377*, 245–254. [CrossRef]

48. Ngo, D.T.; Tan, Q.; Wang, B.; Resasco, D.E. Aldol Condensation of Cyclopentanone on Hydrophobized MgO. Promotional Role of Water and Changes in the Rate-Limiting Step upon Organosilane Functionalization. *ACS Catal.* **2019**, *9*, 2831–2841. [CrossRef]

49. Young, Z.D.; Hanspal, S.; Davis, R.J. Aldol Condensation of Acetaldehyde over Titania, Hydroxyapatite, and Magnesia. *ACS Catal.* **2016**, *6*, 3193–3202. [CrossRef]

50. Zhao, L.; An, H.; Zhao, X.; Wang, Y. TiO$_2$-Catalyzed n-Valeraldehyde Self-Condensation Reaction Mechanism and Kinetics. *ACS Catal.* **2017**, *7*, 4451–4461. [CrossRef]

51. Lu, B.; Wang, Z.; Ma, S.; Mao, S.; Chen, Z.; Wang, Y. Spatial charge separation induced new mechanism of efficient C-C coupling by forming ion-pair intermediates. *Chem Catal.* **2021**, *1*, 1449–1465. [CrossRef]

52. Song, R.; Meng, X.; Yu, C.; Bian, J.; Su, J. Oil shale in-situ upgrading with natural clay-based catalysts: Enhancement of oil yield and quality. *Fuel* **2022**, *314*, 123076. [CrossRef]